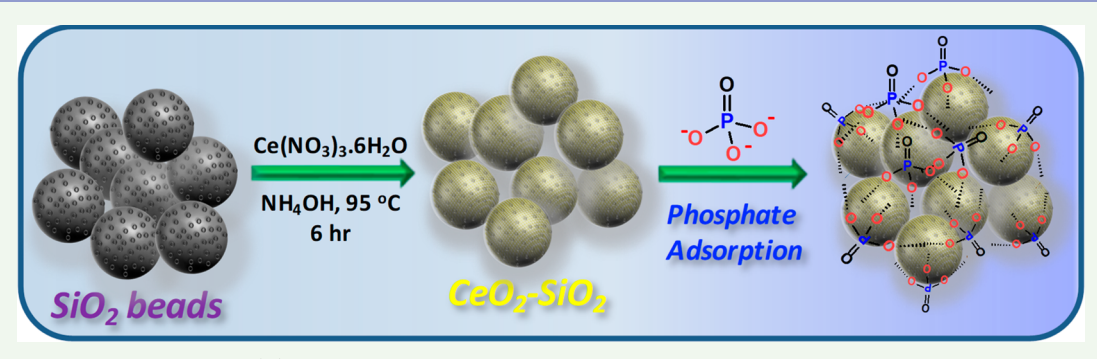
www.acsanm.org

# Recyclable Adsorbents Based on Ceria Nanostructures on Mesoporous Silica Beads for the Removal and Recovery of **Phosphate from Eutrophic Waters**

Ali Othman, Peter Vargo, and Silvana Andreescu\*

Department of Chemistry and Biomolecular Science, Clarkson University, Potsdam, New York 13699-5810, United States

Supporting Information



ABSTRACT: While phosphorus (P) is an essential nonrenewable resource and a key nutrient for agricultural production, its excessive accumulation in the environment can cause overgrowth of water plants and algal blooms that produce dangerous toxins and create "dead zones" in the body of water, leading to eutrophication. Main approaches to remove P in its most abundant and stable form, phosphate  $(PO_4^{\ 3})$ , involve the use of carbon-based adsorbents that are relatively nonspecific, have limited sorption capacity, and cannot be used to recover this critical resource. Herein, we report a ceria (CeO2)-based adsorbent that has the capability to rapidly and reversibly capture PO<sub>4</sub><sup>3-</sup> enabling its further recovery for potential reuse. The adsorbent consists of ceria nanoparticles patterned on mesoporous silica (CeO<sub>2</sub>-SiO<sub>2</sub>), which can bind PO<sub>4</sub><sup>3-</sup> through ion exchange and Lewis-acid based interactions. The adsorbent shows excellent sorption/desorption capability of up to 110 mg/g with 99% removal within 60 min. The adsorbent maintained high removal efficiency over a pH ranging from 4 to 8.5 and showed no significant effect to common coexisting anions, indicating high selectivity for PO<sub>4</sub><sup>3-</sup>. A procedure to regenerate the adsorbent by hydrogen peroxide (H<sub>2</sub>O<sub>2</sub>) treatment was developed which enabled the reuse of the adsorbent for up to six cycles and the recovery of the  $PO_4^{3-}$ . The designed  $CeO_2$ -SiO<sub>2</sub> provides an example of regenerable high-performance adsorbents based on ceria chemistry that can be used to control and manage  $PO_4^{3-}$  levels in environmental water systems to address issues related to eutrophication.

KEYWORDS: ceria-based adsorbent, phosphate, regeneration, adsorbent selectivity, redox, eutrophication, environmental remediation, batch adsorption

# 1. INTRODUCTION

Water management is a challenging problem at local and global levels. The availability of clean and safe water resources is essential for ensuring the water needs for human consumption and natural ecosystems. Industrial activities and agricultural practices can affect water quality and impact the nutrient cycle, affecting a variety of processes in the ecosystem, with one of the most altered involving the phosphorus  $(PO_4-P)$  cycle. The use of P-based fertilizers and detergents generate an oversupply of P compounds in inland and coastal waters. A large amount is entering the water circuit through soil leaching from the use of fertilizers or food waste (1 million tons).<sup>3</sup> Excessive P in the environment causes overgrowth of water plants and toxic algal blooms and creates "dead zones" in the body of water, resulting in changes of habitats and raising drinking water treatment costs. It is estimated that about 40% of rivers and

water streams in the US are P rich, leading to poor water quality and an inability to support aquatic life,4 making P pollution a serious challenge.

Given the essential role of P in the environment, it is critical to develop solutions to improve the overall management of the P-cycle and ensure an overall nutrient balance, while preserving the beneficial uses of P for agricultural food production. Therefore, effective strategies to remove the excess of P are needed to prevent algal growth and minimize cyanotoxin formation. Removal of P is also needed to create a source of recycled P-compounds. Previous work has demonstrated the use of adsorbent for the removal of P species, particularly the

Received: August 7, 2019 Accepted: October 7, 2019 Published: October 7, 2019



most abundant form as inorganic phosphate (PO<sub>4</sub><sup>3-</sup>), using materials such as activated carbon, <sup>6</sup> zirconium hydroxide <sup>7</sup> and zirconia-functionalized graphite oxide, seolites, amorphous calcium carbonate, and iron(III) oxides. While these adsorbents have shown good performance for phosphate removal, they lack selectivity, do not allow for the recovery of PO<sub>4</sub><sup>3-</sup> and cannot be reused.

Ceria (CeO<sub>2</sub>) and CeO<sub>2</sub>-based adsorbents have received great interest as promising adsorbent for water treatment. The high surface charge density, rich functionalities, and the high affinity of surface hydroxyl groups facilitate rapid formation of cerium-ion (e.g., phosphate, arsenic, etc.) complexes to their surface, 12-14 making them effective adsorbents for environmental remediation. Few recent reports described the potential of CeO<sub>2</sub> in nanoparticles<sup>15</sup> and hydrous forms loaded on porous silica microsphere (Ce-SiO<sub>2</sub>)<sup>16</sup> and Fe<sub>3</sub>O<sub>4</sub>@SiO<sub>2</sub> magnetic nanoparticles<sup>17</sup> as potential candidates for the removal of PO<sub>4</sub><sup>3-</sup>. While PO<sub>4</sub><sup>3-</sup> adsoption on CeO<sub>2</sub> has been reported, none of these studies address evident needs to regenerate and recycle the sorbent.

Herein, we describe a recyclable CeO2-based adsorbent that has the capability to catch and release PO<sub>4</sub><sup>3-</sup>, enabling its recovery, and the reuse of the adsorbent. To design the adsorbent, we use the high binding ability of CeO2 nanostructures for PO<sub>4</sub><sup>3-</sup>, by forming cerium phosphate complexes at the CeO2 surface. To fabricate the adsorbent, CeO<sub>2</sub> nanostructures were grafted on mesoporous SiO<sub>2</sub>, which can be conveniently used in the fabrication of membranes and filters or as packing media for separation columns. The high surface area and affinity of CeO<sub>2</sub> for these compounds make them suitable adsorbents for PO<sub>4</sub><sup>3-</sup> removal and recovery. This is the first study demonstrating the regenerability of CeO2based materials as reusable adsorbents for the selective PO<sub>4</sub> removal and environmental remediation applications.

## 2. EXPERIMENTAL SECTION

**2.1. Materials.** The cerium(III) nitrate hexahydrate  $(Ce(NO_3)_3)$ 6H<sub>2</sub>O, 99%) was of analytical grade and was purchased from Sigma-Aldrich. Silica gel (60-200 Mesh) and sodium sulfate were purchased from J.T. Baker. Dipotassium hydrogen phosphate (K2HPO4, >99.9%), sodium chloride, sodium flouride were purchased from Fisher. Ascorbic acid was purchased from LabChem. Ammonium molybdate (para) tetrahydrate ((NH<sub>4</sub>)<sub>6</sub>Mo<sub>7</sub>O<sub>24</sub>·4H<sub>2</sub>O), antimony potassium tartrate hydrate (C<sub>8</sub>H<sub>4</sub>K<sub>2</sub>O<sub>12</sub>Sb<sub>2</sub>·H<sub>2</sub>O, 98%), and sodium perchlorate were purchased from Alfa Aesar. Stock solutions were all prepared with ultrapure water.

2.2. Preparation of Adsorbent. The adsorbent material (i.e., CeO<sub>2</sub>-SiO<sub>2</sub>) was prepared via coating silica gel beads with CeO<sub>2</sub> nanostructures. Seeding of CeO2 onto SiO2 was achieved using a modified synthesis procedure reported in literature.<sup>18</sup> Two hundred milliliters of Ce(NO<sub>3</sub>)<sub>3</sub>·6H<sub>2</sub>O, 0.2 M was preheated to 95 °C and then was mixed with 10 g of silica gel into 20 mL of H<sub>2</sub>O. Afterward, 300 mL of NH<sub>4</sub>OH (0.2 M) was added under vigorous stirring. Then the mixture was kept at this temperature and stirred for 6 h. The product was filtered and washed thoroughly with water to eliminate unbound cerium nitrate or ceria. Finally, the product was dried at 80 °C overnight and placed in a capped container.

2.3. Instrumentation. The spectroscopic analysis was performed using UV-vis spectrophotometer (UV-2401PC, Shimadzu) (1.5 mL methacrylate cuvettes, Fisher Sci.) and Fourier transform infrared (FTIR) equipped with Attenuated total reflectance (ATR-FTIR) (iS10 FT-IR, ATR diamond crystal, Thermo Nicolet). For surface charge measurement, zeta ( $\zeta$ ) potential of the adsorbent solutions using Zeta PALS analyzer (Brookhaven) were measured at 25 °C with n = 5. Thermogravimetric analysis (TGA) of the adsorbent was performed using an Exstar TG/Differential Thermal Analyzer (DTA) 6200 analyzer, (Seiko). All tests were performed with a heating rate of 20 °C/min under N<sub>2</sub> atmosphere in the range of 30-600 °C. To study the elemental composition and oxidation state of species at the surface of the adsorbents, X-ray photoelectron microscopy (XPS) (SSX-100, Surface Science (ESCA)) was used equipped with a monochromatic Al K $\alpha$  X-ray source (1486.6 eV) at 1 mm diameter beam size, a 55° emission angle, an operating pressure of  $\sim 2 \times 10^{-1}$ Torr, 150 V pass energy for wide/survey scans, and 50 V for highresolution scans. For charge neutralization of nonconductive samples a flood gun was used. The surface morphology and chemical composition were evaluated using field emission scanning electron microscopy (FE-SEM), (JEOL JSM-7400F) equipped with an energydispersive X-ray analysis (EDS) using a. The samples were applied on carbon tape, vacuum-dried, and coated with gold (Au)/palladium (Pd) film (60:40%) for 40 s for conductivity purposes. Highresolution transmission electron microscopy (HRTEM), (JEOL JSM-2010) was further used for morphology analysis. The samples were deposited on a TEM copper grid (obtained from Ted Pella) and dried under vacuum before analysis.

To evaluate the crystallinity of the adsorbents a D-8 X-ray diffractometer (Bruker), using Cu K $\alpha$ 1 radiation source was used. To study the surface area, nitrogen (N2) adsorption/desorption isotherms using Autosorb IQ automated gas sorption analyzer (Quantachrome) were carried out. Results were calculated using the Brunauer-Emmett-Teller (BET) method at 77 K. The pore size distribution were obtained based on the quenched solid density functional theory (QSDFT). Survey samples were degassed at 100 °C for 20 h prior to the measurements.

2.4. Phosphate Isotherm Adsorption Study. The PO<sub>4</sub><sup>3-</sup> adsorption capacity by the CeO2-SiO2 adsorbent was measured by using a batch adsorption methodology. Working  $PO_4^{\ 3-}$  solutions were prepared from a stock solution of  $PO_4^{\ 3-}$  (1000 mg/L) prepared in DI water. Briefly, 2 mg/mL of CeO<sub>2</sub>-SiO<sub>2</sub> was added into centrifugation tubes containing PO<sub>4</sub><sup>3-</sup> at a concentration range of 0.5-100 mg/L. Thereafter, the centrifugation tubes were placed in an automatic shaker (Vari-Mix, Thermolyne) and mixed for 60 min. The sample tubes were further centrifuged and filtered using 0.2  $\mu$ m filters. Finally, supernatants were taken and analyzed by the molybdenum blue (MB) method for  $PO_4^{3-}$  concentration.  $^{19}$  SiO<sub>2</sub> beads were tested as control using the same procedure. The  $PO_4^{3-}$  removal effeciency (q%) and the amount of adsorbed PO<sub>4</sub><sup>3-</sup> was calculated using

$$q\% = \frac{(C_{\rm i} - C_{\rm e})}{C_{\rm i}} \times 100 \tag{1}$$

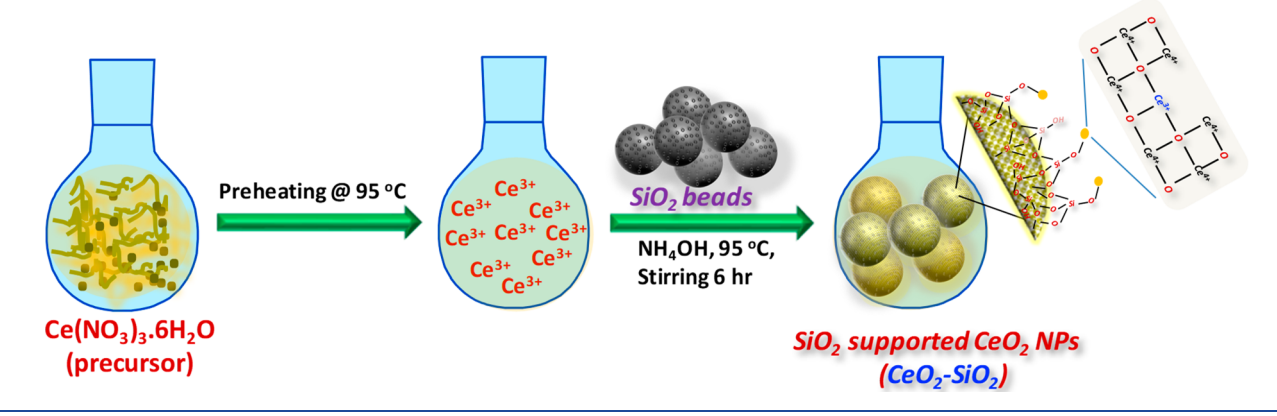
$$q_{\rm e} = \frac{(C_{\rm i} - C_{\rm e})V}{W} \tag{2}$$

where  $q_e$  is the adsorbed PO<sub>4</sub><sup>3-</sup> onto the CeO<sub>2</sub>-SiO<sub>2</sub> surface (mg/g), C<sub>i</sub> and C<sub>e</sub> are the initial and equilibrium concentrations of PO<sub>4</sub> (mg/L) in solution, V is the volume of the sample (L), and W is the weight of  $CeO_2$ -SiO<sub>2</sub>, (g).

**2.5. Kinetic Study of PO\_4^{3-} Adsorption.** The kinetic of  $PO_4^{3-}$ adsorption was studied by batch experiments at different incubation times. In these experiments, CeO<sub>2</sub>-SiO<sub>2</sub> (2 mg/mL) was added to centrifuge tubes containing 17.5 mg/L of PO<sub>4</sub><sup>3-</sup> placed on a shaker (Vari-Mix, Thermolyne) and mixed for different time periods from 1 to 60 min at room temperature. The concentrations were optimized based on the molybdenum blue method. After incubation, the supernatant was analyzed for residual PO<sub>4</sub><sup>3-</sup> concentration.

2.6. Adsorbent Dosage and pH Effects. The CeO2-SiO2 dosage was optimized by testing amounts of adsorbent in the range of (0.5, 1, 2.5, 5, and 10 mg/mL), The adsorbent was exposed to PO<sub>4</sub><sup>3-</sup>(17.5 mg/L) mixed and placed on shaker for 60 min. The samples were then centrifuged and filtered and the amount of PO<sub>4</sub><sup>3</sup> was analyzed using the  $\widetilde{MB}$  method for  $PO_4^{\ 3-}$  detection. The pH range investigated was between 4 and 10. Solutions of different pH values were obtained by adjusting the pH of PO<sub>4</sub><sup>3-</sup> solutions (50 mL of 17.5 mg/L) with 0.1 M NaOH or HCl. Two mg/mL of CeO<sub>2</sub>-SiO<sub>2</sub> adsorbent were added to the PO<sub>4</sub><sup>3-</sup> solutions of different pH

Scheme 1. Schematic Representing the Functionalization of SiO<sub>2</sub> with CeO<sub>2</sub> NPs



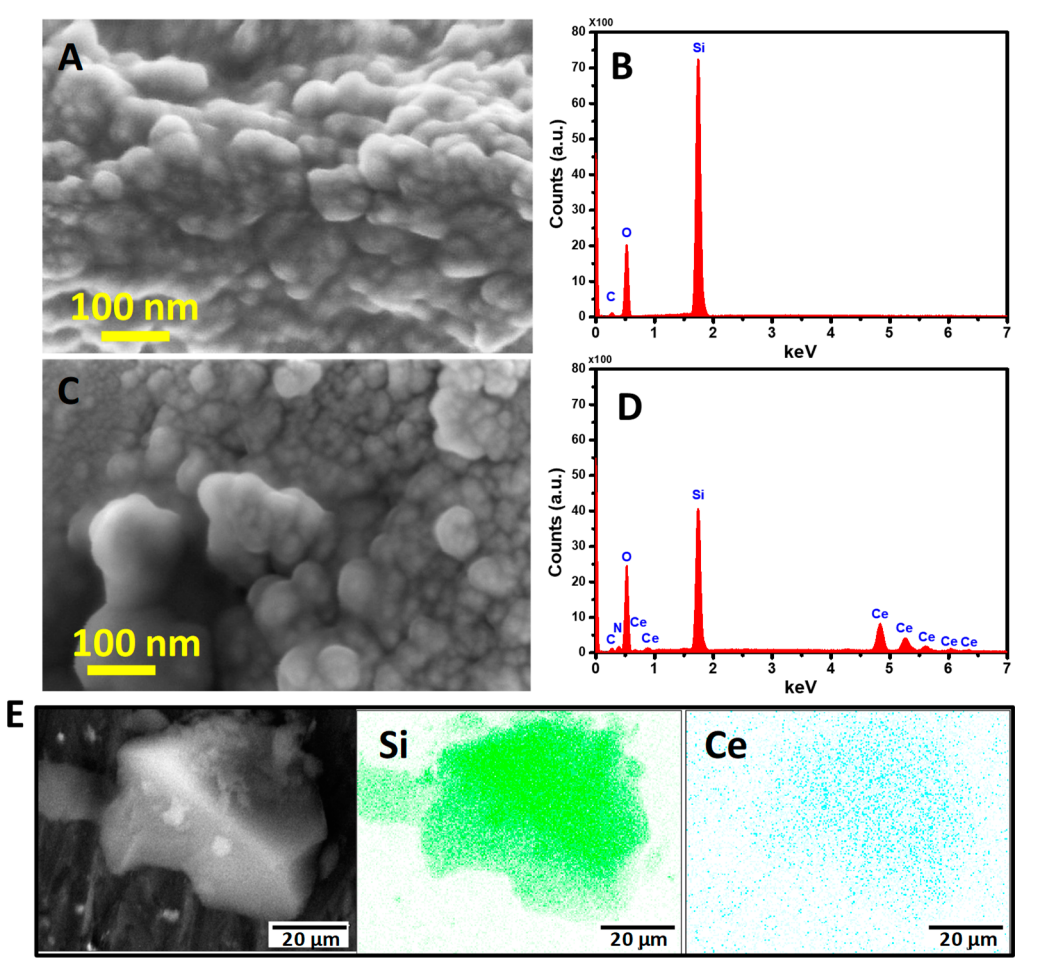


Figure 1. SEM images of  $SiO_2$  beads (A) and  $CeO_2$ – $SiO_2$  adsorbent (C) with their corresponding EDS analysis (B and D, respectively). (E) The corresponding elemental mapping of  $CeO_2$ – $SiO_2$  adsorbent.

values, and the adsorbed  $PO_4^{3-}$  was determined using the same procedure as in the adsorption study.

**2.7. Recyclability and Regeneration.** Regeneration of the adsorbent was achieved by washing with  $H_2O_2$ , which competitively displaces the adsorbed  $PO_4^{\ 3-}$ . To regenerate the  $CeO_2-SiO_2$ , the spent adsorbents were added to  $H_2O_2$  solution (0.1 M) and then mixed on a shaker for 1 h. The  $CeO_2-SiO_2$  was washed with DI water, and then centrifuged and dried at 100 °C to decompose the adsobed Ce-peroxide and regenerate the adsorbent. Thereafter, six repetitive experiments of  $PO_4^{\ 3-}$  adsorption/desorption cycles for were carried to evaluate the reusability of the adsorbent.

Note: All experiments were carried out with solutions at a pH 7.0 (except for the pH study), at room temperature. The calibration curve for  ${\rm PO_4}^{3-}$  using the MB method was developed based on three replicates (n=3).

## 3. RESULTS AND DISCUSSION

**3.1.** Adsorbent Characterization. Silica beads offer a strongly hydrophobic environment with the ability to entrap and anchor metal oxides in/onto its microstructure producing a highly uniform conjugate. In particular,  $CeO_2$  is known to form strong Ce-O-Si bonds with the  $SiO_2$  surface. By

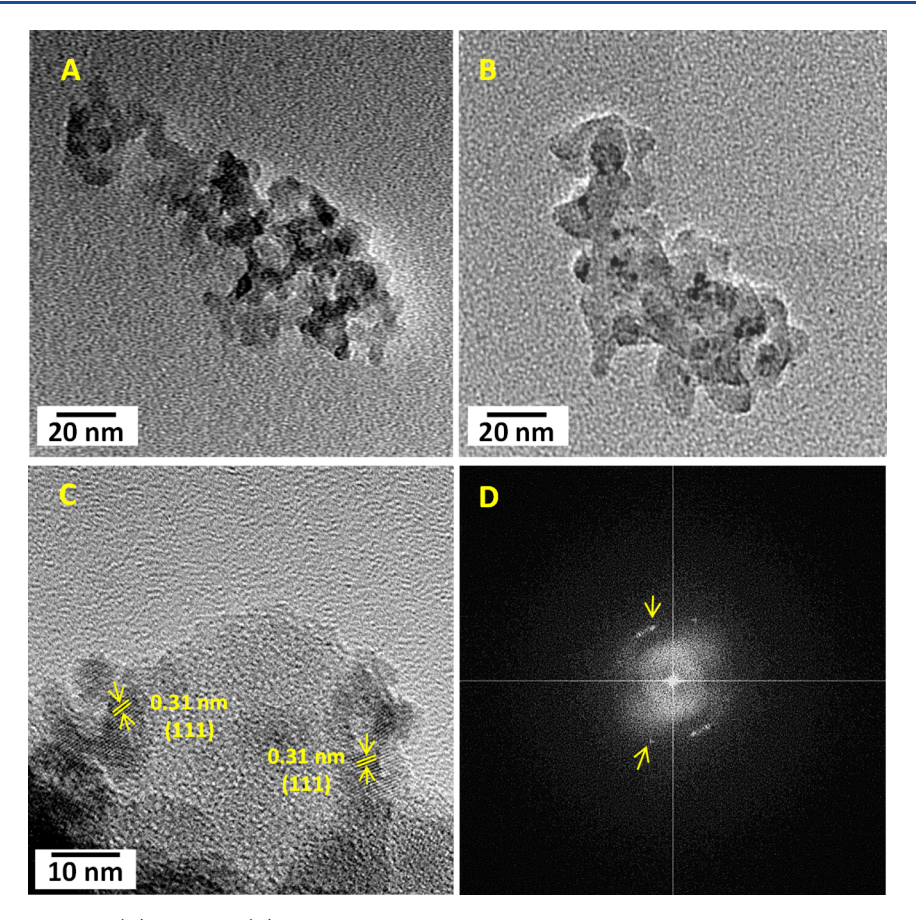


Figure 2. HR-TEM migrographs of (A)  $SiO_2$  and (B)  $CeO_2$ - $SiO_2$  adsorbent. Panels C and D are the HRTEM images of  $CeO_2$ - $SiO_2$  adsorbent at high magnification with the corresponding fast Fourier transformation (FFT) pattern.

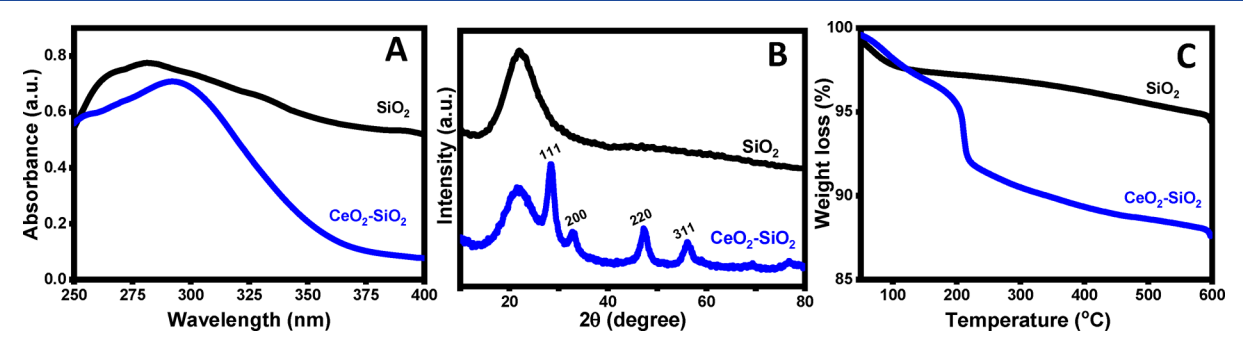


Figure 3. Chemical structure characterization of the CeO2-SiO2 adsorbent: (A) UV-vis spectra, (B) XRD patterns, and (C) TGA profiles.

depositing a nanostructured  $CeO_2$  on the  $SiO_2$  beads, we create a high surface area structure with high density capturing sites for  $PO_4^{\ 3^-}$  species. It is known that  $PO_4^{\ 3^-}$  can interact strongly with  $CeO_2$  and promote  $CePO_4$  formation. The procedure for preparing the  $CeO_2$ – $SiO_2$  adsorbent consists in direct  $CeO_2$ NPs precipitation onto the  $SiO_2$  surface as illustrated in Scheme 1. The pH value of the as-prepared  $CeO_2$ – $SiO_2$  has a point of zero charge (pzc) at pH 4.1, higher than the pH associated with the pzc of the initial  $SiO_2$  beads (3.6) (Figure S1). The change in  $\zeta$ /pH evolution is the first confirmation of a successful  $CeO_2$  coating of the silica beads.

The morphology and the chemical composition of the adsorbent were assessed by SEM and EDS analysis. The SEM images of both SiO<sub>2</sub> and CeO<sub>2</sub>–SiO<sub>2</sub> (Figure 1A and C) show that the morphology of the material is maintained after functionalization. The chemical composition was confirmed by

EDS analysis (Figure 1B and D). As compared to the EDS spectrum of SiO<sub>2</sub>, the CeO<sub>2</sub>–SiO<sub>2</sub> shows the presence of Ce indicating the successful modification of SiO<sub>2</sub> with CeO<sub>2</sub>. Additionally, the corresponding elemental (Si and Ce) mapping of CeO<sub>2</sub>–SiO<sub>2</sub> adsorbent (Figure 1E) illustrates a homogeneous distribution of CeO<sub>2</sub> over the SiO<sub>2</sub> surface.

The surface properties and the porosity analysis of the  $SiO_2$  beads and the  $CeO_2-SiO_2$  adsorbent are shown in (Figure S2) the parameters are displayed in Table S1. The  $N_2$  adsorption/desorption isotherms exhibit a similar type IV curve for both materials:  $SiO_2$  and  $CeO_2-SiO_2$  beads. The specific surface area ( $S_{BET}$ ) value of  $SiO_2$  decreased slightly from 287.5 ( $SiO_2$ ) to 274.0 m²/g ( $CeO_2-SiO_2$ ). The values of the pore volume also decreased from 1.033 ( $SiO_2$ ) to 1.025 cm³/g ( $CeO_2-SiO_2$ ). These results demonstrate that the  $CeO_2-SiO_2$  maintained a mesoporous structure after functionalization.

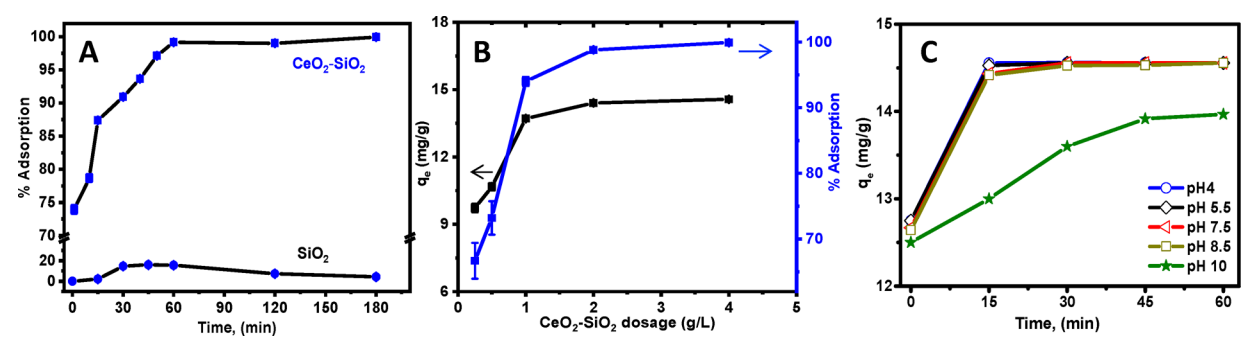


Figure 4. Effect of (A) contact time, (B) adsorbent dosage, and (C) pH on the adsorption capacity of  $PO_4^{3-}$ .  $[PO_4^{3-}]_{ini} = 17.5 \text{ mg/L}$ . n = 3.

Surface modification of  $SiO_2$  by  $CeO_2$  was further studied by HR-TEM analysis. Figure 2 shows a spherical shape which is maintained after functionalization. The HR-TEM of the  $CeO_2$ – $SiO_2$  adsorbent at high magnification (Figure 2C) confirms the presence of  $CeO_2$  NPs with a spherical-like shape structure distributed on the  $SiO_2$ . The image also shows fine particles in the range of average size of 5–15 nm uniformly distributed in the sample and possess a lattice fringe characteristics of a d-spacing of 0.31 nm attributed to the (111) facet of fcc of  $CeO_2$  NPs. The fast Fourier transformation (FFT) data (Figure 2D) are consistent with a diffraction pattern of fcc crystals in the (111) planes.

Further characterization was performed by UV-vis, XRD, and TGA (Figure 3) techniques. The UV-vis spectrum of SiO<sub>2</sub> (Figure 3A) shows an absorbance peak at 280 nm. After CeO<sub>2</sub> was precipitated onto the SiO<sub>2</sub> beads, a new absorbance peak with a maximum wavelength at ~300 nm is present. This peak is a well-known characteristic of CeO2, confirming its presence on the SiO<sub>2</sub> surface. The PXRD pattern of the SiO<sub>2</sub> (Figure 3B)shows a broad peak around  $2\theta = 22^{\circ}$  associated with an amorphous structure of this material. After introducing CeO<sub>2</sub>, the intensity of this peak is reduced, which is associated with the appearance of  $2\theta$  diffraction peaks at  $28.4^{\circ}$ ,  $32.8^{\circ}$ , 47.2°, and 56.1°. These peaks are characteristics of the 111, 200, 220, and 311 planes, assigned to the face-centered cubic (fcc) CeO<sub>2</sub> structure.<sup>22</sup> The interplanar spacing and the crystallite size of the CeO<sub>2</sub> estimated by considering the (111) plane were 0.31 and 4.4 nm, according to the Scherrer equation. These spectroscopic and structural data confirm the presence and the nanosized feature of the CeO2 in agreement with the HR-TEM data. The TGA profiles of both SiO<sub>2</sub> and  $CeO_2$ -SiO<sub>2</sub>(Figure 3C) show an initial loss of ~2.5% in the range of 50-150 °C because of the loss of the adsorbed water. An extra slight weight loss of ~1.5% up to 600 °C was observed which can be attributed to the condensation of silanol groups.<sup>23</sup> For the CeO<sub>2</sub>-SiO<sub>2</sub>, a ~9% weight loss at 150-250 °C was observed. Since the synthesized CeO<sub>2</sub> contains hydrated ceria onto the surface, this loss is due to the elimination of water.<sup>24</sup>

Surface modification was further investigated using ATR-FTIR and XPS techniques. The ATR-FTIR spectra of bare and CeO<sub>2</sub>-coated SiO<sub>2</sub> shown in (Figure S3A) exhibits bands at 960 and 1632 cm<sup>-1</sup> corresponding to the (Si–O or Ce–O) vibrations in bare SiO<sub>2</sub> and CeO<sub>2</sub>–SiO<sub>2</sub>, respectively.<sup>25</sup> The very intense and broad band at ~1110 cm<sup>-1</sup> and the band at 805 cm<sup>-1</sup> both correspond to the Si–O–Si stretching vibration.<sup>26</sup> The small shoulder at 960 cm<sup>-1</sup> is assigned to the stretching of (Si–OH or Ce–OH).<sup>27</sup> For CeO<sub>2</sub>–SiO<sub>2</sub>, these peaks shift to lower wavenumbers due to the insertion of

CeO<sub>2</sub> in the silica framework, with formation of Ce-O-Si bonds. In addition, new peaks at 1385 and 1462 cm<sup>-1</sup> are also seen after functionalization, associated with the Ce-O-Ce and Ce-OH vibrations.<sup>28</sup>

XPS analysis (Figure S3B and C) in the range of 0-1200 eV shows the Si 2p signal in both SiO<sub>2</sub> and CeO<sub>2</sub>–SiO<sub>2</sub> samples with the signal shifted from 104.7 for SiO<sub>2</sub> to 103.8 eV for CeO<sub>2</sub>–SiO<sub>2</sub>. This 0.9 eV shift toward lower binding energy could be explained by the interaction of Si with Ce ions. As expected, Ce 3d was absent in the SiO<sub>2</sub> sample and observed only in the CeO<sub>2</sub>–SiO<sub>2</sub> sample as can be seen from the (Figure S3B and C), respectively. The Ce 3d spectrum of CeO<sub>2</sub>–SiO<sub>2</sub>(inset of Figure S3C) showed evidence of a mixed oxidation state (Ce<sup>3+</sup>/Ce<sup>4+</sup>). The peaks at 886 and 906 eV are due to Ce in the 3+ state, while the peaks at 882, 900, and 916 eV are attributed to Ce in the 4+ oxidation state.<sup>29</sup> These results indicate the presence of CeO<sub>2</sub> onto SiO<sub>2</sub> confirming the successful preparation of the CeO<sub>3</sub>–SiO<sub>3</sub> adsorbent.

3.2. Adsorption of  $PO_4^{3-}$  on  $CeO_2$ -SiO<sub>2</sub>.  $CeO_2$  NPs are known for their ability to interact with PO<sub>4</sub><sup>3-</sup> creating cerium phosphate (Ce-PO<sub>4</sub>) at their surface. Therefore, decoration of CeO<sub>2</sub> onto the surface of porous support provides sites for PO<sub>4</sub><sup>3-</sup> adsorption on and within the mesoporous structure, significantly enhancing the adsorption capacity of this material. It was also reported that binding of phosphate anions induces changes in the redox state of CeO<sub>2</sub> (i.e., Ce<sup>3+</sup>/ Ce<sup>4+</sup>) through coordination to cerium cations on Ce<sup>3+</sup>-rich CeO<sub>2</sub> without affecting the crystal structure of CeO<sub>2</sub>. 30,31 A recent computational study reports a preferential interaction of PO<sub>4</sub><sup>3-</sup> with Ce<sup>3+</sup> and highlights the role of hydroxyl groups in the phosphate ion adsorption, although it was suggested that the interaction between phosphate (PO<sub>4</sub><sup>3-</sup>) and hydroxyl (OH<sup>-</sup>) groups appear to be minimal and independent of the OH concentration.<sup>21</sup> However, CeO<sub>2</sub> NPs could suffer from agglomeration because of the van der Waals interactions or leaching through filtration or separation. As a result, the sorption capacity, selectivity, and mechanical strength are significantly decreased making them less feasible for use in water systems. To overcome this disadvantage, CeO<sub>2</sub> NPs were decorated on mesoporous SiO2 beads, which are commonly used as packing or filtration material. The effect of solution pH, contact time, and chemical composition was studied further to understand the effect of these parameters on PO<sub>4</sub><sup>3-</sup> adsorption by CeO<sub>2</sub>-SiO<sub>2</sub>.

3.2.1. Study of the Contact Time Effect on PO<sub>4</sub><sup>3-</sup> Adsorption. Incubation times ranging between 1 and 180 min were tested to determine the optimum adsorption of PO<sub>4</sub><sup>3-</sup>. Batch sorption experiments were used in these studies. For comparison, PO<sub>4</sub><sup>3-</sup> adsorption on the CeO<sub>2</sub>-SiO<sub>2</sub> was

ACS Applied Nano Materials Article

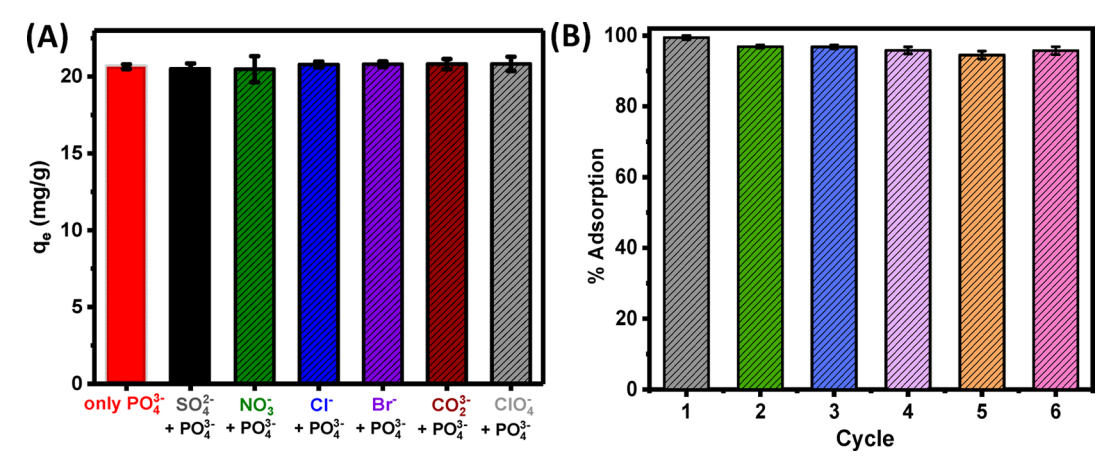


Figure 5. (A) Effect of coexisting anions on  $PO_4^{3-}$  adsorption by  $CeO_2-SiO_2$ .  $[PO_4^{3-}]_{ini} = [Anion]_{ini} = 25 \text{ mg/L}$ , time = 60 min. (B) Recyclability test on  $PO_4^{3-}$  adsorption by  $CeO_2-SiO_2$ .  $[PO_4^{3-}]_{ini} = 35 \text{ mg/L}$ .

compared with that obtained on unmodified  $SiO_2$  as a control. Bare  $SiO_2$  (Figure 4A) showed almost no  $PO_4{}^{3-}$  adsorption, while the  $CeO_2-SiO_2$  displayed a fast time dependent adsorption process. The % amount of  $PO_4{}^{3-}$  adsorbed by  $CeO_2-SiO_2$  increased with time from 74% due to increase of the contact between the  $PO_4{}^{3-}$  and the adsorbent until it reached equilibrium at 60 min, with more than 99% adsorption. Extending the contact time above 60 min did not show a significant change in the amount of adsorbed  $PO_4{}^{3-}$ , indicating that the adsorption phase reached equilibrium. This behavior suggests that the kinetics is fast at the earlier stages of the adsorption process due to the accessibility of the active binding sites, followed by slow kinetics due to blocking of binding sites of  $CeO_2-SiO_2$  by  $PO_4{}^{3-}$  species.  $^{32}$ 

3.2.2. Adsorbent Dosage Effect.  $CeO_2-SiO_2$  concentrations in 0.25–4 g/L range were tested to determine the adsorption capacity of  $PO_4^{3-}$  (Figure 4B). According to the results of the batch adsorption experiments, the equilibrium between the surface adsorption and adsorbent concentration was reached at 2 g/L which corresponds to an adsorption capacity of up to 99% with  $q_e$  of 14.6 mg/g.

3.2.3. pH Effect. One of the key factors that play a role in the adsorption process is the pH of the solution, since the pH affects the surface charge of both the adorbent and adsorbate. The effect of pH on the adsorption capacity of PO<sub>4</sub><sup>3-</sup> by CeO<sub>2</sub>–SiO<sub>2</sub> was studied in the pH range of 4 to 10. Results in Figure 4C show that the removal of PO<sub>4</sub><sup>3-</sup> by CeO<sub>2</sub>–SiO<sub>2</sub> occurs at a similar rate for pH values between 4 and 8.5, with a sligh enhancement at acidic pH. When the pH exceeded 10, the adsorption capacity decreased. This is in agreement with previous reports indicating that higher pH values tend to facilitate PO<sub>4</sub><sup>3-</sup> desorption. 33,34</sup> The lack of pH dependency demonstrates that the adsorption process is independent of the hydroxyl concentration in this pH range and the P–CeO<sub>2</sub> are very stable over a wide range of pH.

**3.3.** Adsorption Study. 3.3.1. Adsorption Isotherm Study. Adsorption isotherms describing the relationship between the amount of the  $PO_4^{3-}$  adsorbed by the  $CeO_2-SiO_2$  were then assessed. The amount of the adsorbed  $PO_4^{3-}$  by the  $CeO_2-SiO_2$  was calculated using eq 2 The Langmuir and Freundlich isotherm models were used to calculate the adsorption parameters by applying eqs 3 and 4. The Langmuir model is applicable when the surface is energetically homogeneous and the extent of adsorbate coverage is limited

to a monolayer. For accurate representation of the equilibrium data, the nonlinear Langmuir model isotherm form was applied.

$$\begin{split} &\frac{C_{\rm e}}{q_{\rm e}} = \frac{1}{K_{\rm L}q_{\rm m}} + \frac{C_{\rm e}}{q_{\rm m}} \text{ (linear form)} \\ &q_{\rm e} = \frac{q_{\rm m}K_{\rm L}C_{\rm e}}{1+K_{\rm L}C_{\rm e}} \text{ (nonlinear form)} \end{split} \tag{3}$$

where  $q_{\rm m}$  in (mg/g) is the maximum adsorption capacity and  $K_{\rm L}$  represents the Langmuir adsorption constant, associated with the adsorption bonding energy (or the affinity of the binding sites (L/mg)). The Freundlich model describes an adsorption process when the heterogeneous surface of an adsorbent is available. The adsorbate coverage is limited to a multilayer and adsorption sites are energetically not equal. The Freundlich isotherm model is expressed as

$$\log q_{\rm e} = \log K_{\rm f} + \frac{1}{n} \log C \text{ (linear form)}$$

$$q_{\rm e} = K_{\rm f} C_{\rm e}^{1/n} \text{ (nonlinear form)}$$
(4)

where  $K_{\rm f}$  is the Freundlich constant associated with the adsorption capacity and 1/n indicates the extent of adsorption favorability.

Experimental data and the nonlinear fitted equilibrium curves using the nonlinear forms of Langmuir and Freundlich equilibrium isotherms models are shown in Figure S4. The nonlinear Langmuir isotherm exhibited a good fit with a correlation coefficient of  $(R^2=0.99)$ . The maximum adsorption capacity  $(q_{\rm m})$  of  $PO_4^{3-}$  onto  $CeO_2$ – $SiO_2$  is high with a value of 110 mg/g. The nonlinear fitting of the isotherm data of  $CeO_2$ – $SiO_2$  using the Freundlich model also exhibited a good fit with a correlation coefficient of  $(R^2=0.96)$ . In addition, the values of 1/n is <1, indicating a favorable adsorption of  $PO_4^{3-}$  on  $CeO_2$ – $SiO_2$ . The parameters calculated by using the nonlinear forms of Langmuir and Freundlich models are tabulated in Table S2. These results suggest that the Langmuir model more favorably describe the  $PO_4^{3-}$  adsorption behavior onto  $CeO_2$ – $SiO_2$ .

3.3.2. Adsorption Kinetics. The adsorption mechanism was further investigated by applying the pseudo-first-order and pseudo-second-order kinetics models to fit the experimental data according to eqs 5 and 6

ACS Applied Nano Materials Article

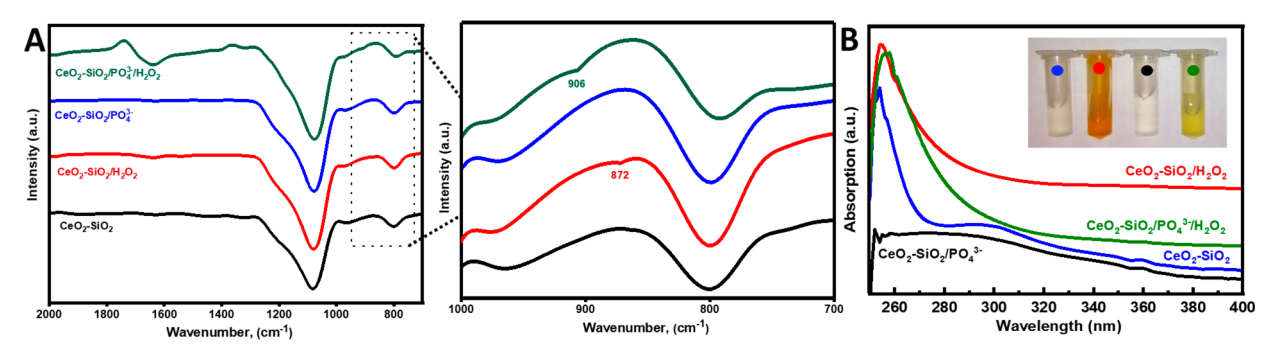


Figure 6. (A) ATR-FTIR with the expanded region (700–1000 cm<sup>-1</sup>) and (B) UV–vis spectra with the inset of the color response of untreated and treated  $CeO_2$ –SiO<sub>2</sub> and  $CeO_2$ –SiO<sub>2</sub>/PO<sub>4</sub><sup>3-</sup> with H<sub>2</sub>O<sub>2</sub>.

pseudo-first-order kinetics model

$$\ln(q_{e} - q_{t}) = \frac{\ln q_{e} - K_{l}t}{2.303} \text{ (linear form)}$$

$$q_{t} = q_{e}(1 - e^{-K_{l}t}) \text{ (nonlinear form)}$$
(5)

pseudo-second-order kinetics model

$$\frac{t}{q_{\rm t}} = \frac{1}{K_2 q_{\rm e}^2} + \frac{t}{q_{\rm e}} \text{ (linear form)}$$

$$q_{\rm t} = \frac{K_1 q_{\rm e}^2 t}{1 + K_1 q_{\rm e} t} \text{ (nonlinear form)}$$
(6)

In the present work, the kinetics study was performed at different  $PO_4^{3-}$  adsorption times by employing the nonlinear forms of pseudo-first- and second-order kinetics. According to the regression data presented in Figure S5 and Table S3, the calculated equilibrium adsorption capacity  $(q_e)$  values are 14.2 and 15.3 mg/g for the pseudo-first-order and pseudo-second-order models, respectively. In addition, the correlation coefficient  $(R^2)$  of the pseudo-first- and pseudo-second-order models are 0.52 and 0.86, respectively. These suggest that the pseudo-second-order model offers a satisfactory adsorption kinetic fitting, indicating that the chemical adsorption mechanism (i.e., chemisorption) is the rate controlling step, and consequently, it may involve chemical valence forces through sharing or exchanging electrons.<sup>35</sup>

**3.4. Interference Study.** To study the effect of the coexisting ions on  $PO_4^{3-}$  adsorption, several ions that are concurrently present in groundwater and wastewater, such as  $SO_4^{2-}$ ,  $NO_3^{-}$ ,  $Cl^-$ ,  $Br^-$ ,  $CO_2^{3-}$ , and  $ClO_4^{-}$  in 1:1 ratio were investigated (Figure 5A). The results show no significant interference of these ions, demonstrating selectivity of the  $CeO_2$ – $SiO_2$  adsorbent for  $PO_4^{3-}$ .

**3.5. Recyclability and Regeneration.** In the next set of experiments, we examined the possibility of recycling the adsorbent for six consecutive adsorption—desorption cycles by using an ion exchange mechanism with peroxide treatment (Figure 5B). The reaction of  $CeO_2$  with  $H_2O_2$  is known to form stable cerium-oxo and peroxide bonds onto the  $CeO_2$  surface. We used this process to competitively replace the adsorbed  $PO_4^{3-}$  by formation of  $Ce-O_2^{2-}$ , creating a pathway for  $PO_4^{3-}$  recovery. The adsorbed  $O_2^{2-}$  can further be decomposed by slightly heating at 100 °C,  $^{38}$  enabling the reuse of the adsorbent.

The effect of  $H_2O_2$  treatment on the  $CeO_2$ -SiO $_2$  surface was measured by ATR-FTIR and UV-vis after several

consecutive adsorption-desorption cycles. After H<sub>2</sub>O<sub>2</sub> treatment, the solid adsorbent was removed by centrifugation, washing with DI water, and drying under vacum. The ATR-FTIR spectrum (Figure 6A) shows that the CeO<sub>2</sub>-SiO<sub>2</sub> adsorbent treated with H<sub>2</sub>O<sub>2</sub> developed a new peak at 872 cm<sup>-1</sup> that is absent in the spectra of both bare and the PO<sub>4</sub><sup>3</sup>-treated adsorbent. A peak in the same 830-950 cm<sup>-1</sup> region reappears after regeneration of the adsorbent by heating. This peak corresponds to the formation of  $Ce-O_2^{2-}$  complexes onto the CeO2-SiO2 surface formed after H2O2 addition, proving a ligand exchange mechanism on the surface of the  ${\rm CeO_2}$ . To evaluate the regenerative capability of  ${\rm CeO_2}$ – SiO<sub>2</sub> after PO<sub>4</sub><sup>3-</sup> adsorption by H<sub>2</sub>O<sub>2</sub>, untreated and treated adsorbents were also analyzed by UV-vis. When CeO<sub>2</sub>-SiO<sub>2</sub> was exposed to H<sub>2</sub>O<sub>2</sub>, a colorimetric change from colorless to dark yellow/orange was developed. The initial peak position associated with Ce in the UV-vis spectrum shifted to a higher wavelength in the  $H_2O_2$ -treated sample due to  $Ce^{+3}$  to  $Ce^{4+}$  oxidation. When the  $CeO_2$ -SiO<sub>2</sub> with sorbed  $PO_4^{3-}$  was treated with H<sub>2</sub>O<sub>2</sub>, the color intensity decreased slightly and a red shift was noticed (Figure 6B). These findings can be explained by a partial blocking of the CeO<sub>2</sub> surface by PO<sub>4</sub><sup>3-</sup>. The zeta potential measurement (Table S4) of the  $PO_4^{3-}$ exposed to CeO2-SiO2 adsorbent shows a decrease in stability from -18 to -13 mV after H<sub>2</sub>O<sub>2</sub> treatment. This result agrees with the UV-vis data and the regeneration study (Figure 5B) both of which showed decreased adsorption of PO<sub>4</sub><sup>3-</sup> after the first regeneration cycle. There was no significant decrease in the adsorption capacity for the next regeneration cycles; the PO<sub>4</sub><sup>3-</sup> recovery was nearly identical for the remaining five cycles. Overall, these results prove that H2O2 is able to exchange the PO<sub>4</sub><sup>3-</sup> species adsorbed on the adsorbent. On the basis of these results, we can conclude that the adsorbent can be successfully regenerated and reused multiple times. Additionally, the adsorbed PO<sub>4</sub><sup>3-</sup> can be recovered and further

**3.6. Adsorption Mechanism.** To further understand the mechanism of PO<sub>4</sub><sup>3-</sup> adsorption by the CeO<sub>2</sub>–SiO<sub>2</sub> adsorbent, the nature of the chemical species formed at the CeO<sub>2</sub>–SiO<sub>2</sub> surface before and after exposure to PO<sub>4</sub><sup>3-</sup> was studied by ATR-FTIR and XPS analysis. ATR-FTIR spectra after PO<sub>4</sub><sup>3-</sup> adsorption (Figure S6) show significant decrease in the main bands at 960, 1385, 1632, and 3405 cm<sup>-1</sup>, corresponding to the Ce–O and C–O, and O–H stretching and bending vibrations. This indicate that PO<sub>4</sub><sup>3-</sup> ions were successfully replaced with the surface hydroxyl groups of the CeO<sub>2</sub>. Unfortunately, the characteristic bands of P–OH and P=O stretching overlap with the characteristic bands of Si–O–Si

ACS Applied Nano Materials Article

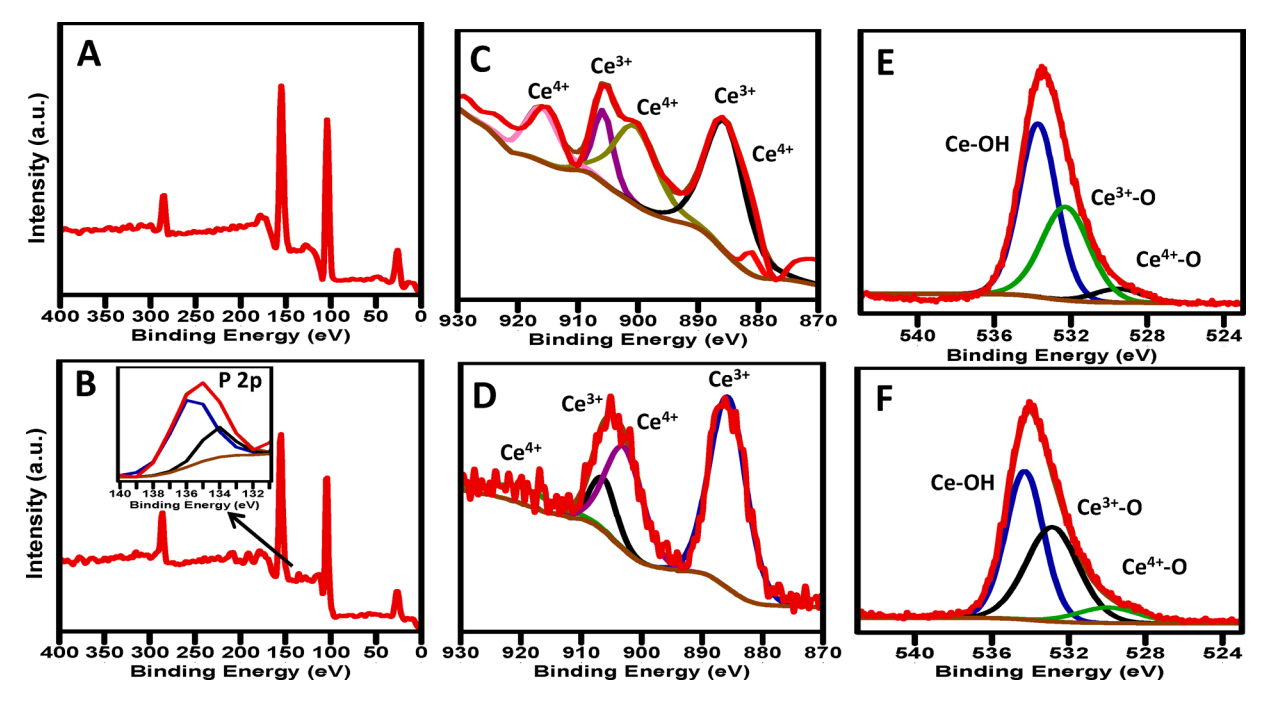


Figure 7. XPS spectra of  $CeO_2$ -Si $O_2$ : (A) Survey, (C) Ce 3d, and (E) O 1s. Panels B, D, and F are the survey, Ce 3d, and O 1s, respectively, of  $CeO_2$ -Si $O_2$ /PO $_4$ <sup>3-</sup> (inset in survey is P 2p spectrum).

(or Ce–O–Si) in the region of 1000–1250 cm<sup>-1</sup>. These significant changes are in line with previous findings indicating a reaction of the PO<sub>4</sub><sup>3-</sup> with the hydroxyls of metal oxide surface<sup>42</sup> and supports a ligand exchange process in which the hydroxyl oxygen on the surface of the metal oxide is replaced by the phosphate oxygen.<sup>43</sup>

Further insight was gained from the XPS analysis of the CeO<sub>2</sub>-SiO<sub>2</sub> adsorbent before and after incubation with PO<sub>4</sub><sup>3-</sup> (Figure 7). The P 2p peak at binding energy of 135 eV was only observed in the sample exposed to PO<sub>4</sub><sup>3-</sup> (Figure 7B). The deconvolution of this peak results into two peaks at 135.6 and 134 eV associated with P(+5) state.<sup>44</sup> The presence of this peak is clear evidence of phosphate species adsorption ( $PO_4^{3-}$ ,  $HPO_4^{2-}$ , and  $H_2PO_4^{-}$ ). The Ce 3d peaks of  $CeO_2$ – $SiO_2$  and CeO<sub>2</sub>-SiO<sub>2</sub>/PO<sub>4</sub><sup>3-</sup> are presented in (Figure 7C and D). The relative concentration of the different Ce species<sup>46</sup> can be evaluated from the peaks area integration associated with the Ce(+3) and Ce(+4) states before and after exposure to  $PO_4^{3-}$ . The relative content of Ce<sup>3+</sup> was found to increase from 48.2% for CeO<sub>2</sub>-SiO<sub>2</sub> to 62.3% for CeO<sub>2</sub>-SiO<sub>2</sub>/PO<sub>4</sub><sup>3-</sup>, supporting the theory that PO<sub>4</sub><sup>3-</sup> binding alters the redox sites of CeO<sub>2</sub>.<sup>3</sup> A Ce<sup>3+</sup> percentage increase as a result of phosphate adsorption was also reported in a recent computational study of PO<sub>4</sub><sup>3-</sup>treated CeO<sub>2</sub> nanoparticles.<sup>21</sup> Next, we analyzed the O 1s XPS spectra (Figure 7E and F). The fitted and deconvoluted O 1s XPS spectrum of CeO<sub>2</sub>-SiO<sub>2</sub> at binding energies of 529.6 and 532.3 eV are assigned to the oxygen bound to Ce<sup>3+</sup> and Ce<sup>4+</sup>, respectively, while that at 533.7 eV is assigned to hydroxyl groups (-OH) or absorbed H<sub>2</sub>O molecules. 47-51 In the O 1s XPS spectrum of CeO<sub>2</sub>-SiO<sub>2</sub>/PO<sub>4</sub><sup>3-</sup>, these three peaks shifted to higher binding energy at 530, 532.8, and 534.4 eV by differences of 0.4, 0.5, and 0.7 eV for the Ce(3+/4+)-O and Ce-(OH/H<sub>2</sub>O), respectively. These changes may be due to surface defects induced by the adsorption of PO<sub>4</sub><sup>3-</sup> and might involve a ligand exchange with the surface hydroxyl groups (-OH) to form Ce-O-P.

At pH below the pzc (pH = 4.1), the adsorbent possesses a positive charge on its surface. The hydroxyl groups of the CeO<sub>2</sub> surface in the aqueous environment provide a site for ligand exchange. This might take place by formation of inner sphere complexes in which the phosphate anions react with Ce<sup>3+</sup> on the structure of the hydroxylated CeO<sub>2</sub> surface, leading to complex formation and the release of hydroxyl anions (OH<sup>-</sup>) from the CeO<sub>2</sub> surface.<sup>34</sup> Furthermore, the pH of the solution containing CeO<sub>2</sub>-SiO<sub>2</sub> increased from 4.9 to 6.9 after PO<sub>4</sub><sup>3-</sup> adsorption, which suggests the replacement of OH by PO<sub>4</sub>3-. Considering the successive pK values of H<sub>3</sub>PO<sub>4</sub> dissociation (2.13, 7.2 and 12.33), in the pH range of our study (4-9), the main species are  $HPO_4^{2-}$  and  $H_2PO_4^{-}$ , as well as PO<sub>4</sub><sup>3-</sup>. In this case, inner-sphere complexation of phosphate ions with the metal (hydro)oxide can lead to monodentate or bidentate phosphorus compounds. 43,52 Since the adsorption process is independent in a pH range from 4 to 8.5 (Figure 4C), where the adsorbent surface is negatively charged, the contribution of electrostatic forces is minimal. These results suggest a mechanism involving ion exchange and Lewis acid-base interactions that implies electron donoracceptor between the hydroxylated CeO2 sites and phosphate anions.<sup>34</sup> Figure 8 provides a schematic illustrating the proposed mechanisms of phosphate adsorption by CeO<sub>2</sub>-SiO<sub>2</sub>.

**3.7. Comparison with Other Adsorbents.** Table 1 summarizes the performance of the  $CeO_2-SiO_2$  with previously reported  $PO_4^{3-}$  adsorbents. The  $CeO_2-SiO_2$  exhibits higher adsorption capacity (110 mg/g) compared with other adsorbents, including several types of metal oxides and activated carbon. The adsorption obtained with our  $CeO_2-SiO_2$  is rapid with up to 99% removal and equilibrium being achieved after 1 h. This is an important factor for increasing treatment efficiency. By incorporating a redox-based regeneration process using  $H_2O_2$ , we presented evidence that the adsorbent can be regenerated and reused for 6 multiple cycles without losing adsorption capacity. While other

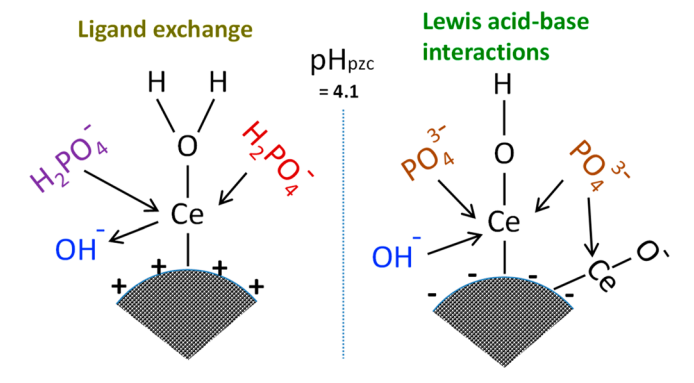


Figure 8. Proposed phosphate adsorption mechanism by the  $CeO_2$ – $SiO_2$  sorbent.

adsorbents such as activated carbon are available, their adsorption capacity is low due to the minimal and nonspecific binding of  ${\rm PO_4}^{3-}$  on carbon materials. In future developments of this technology, this adsorbent could be grafted or incorporated on different materials, such as polymers or graphene composites, or can be used to construct membranes and separation columns to further increase removal efficiency and develop practical systems based on these materials. These results demonstrate very promising characteristics of the  ${\rm CeO_2-based}$  adsorbent to reversibly reuse the adsorbent and remove the bound  ${\rm PO_4}^{3-}$ .

# 4. CONCLUSION

In summary, a  $CeO_2$ – $SiO_2$  adsorbent was synthesized and characterized for the removal of  $PO_4^{\ 3-}$ . The  $CeO_2$ – $SiO_2$  was obtained by grafting nanostructured  $CeO_2$  onto the surface of mesoporous  $SiO_2$  beads through Si-O-Ce bond formation. The modification of  $SiO_2$  with  $CeO_2$  was found to provide enhanced  $PO_4^{\ 3-}$  adsorption of bare  $SiO_2$ , and impart selectivity. The material shows a maximum adsorption capacity of 110 mg/g with 99% removal reached within 1 h. Kinetic models fitted with the experimental batch adsorption data, indicating chemical adsorption as a rate controlling step. Furthermore, the Langmuir model and the analysis of surface properties suggest a monolayer adsorption mechanism involving ion exchange and Lewis acid—base interactions. The process shows high tolerance to changes in pH in the range between pH 4 and 8.5 and the adsorption was selective,

with no interferences from coexisting anions. Results also show that the adsorbent can be regenerated and reused for up to 6 consecutive cycles without a significant decline in performance. The removal efficiency was superior to that of other adsorbents and demonstrates advantages of these materials for use in environmental remediation applications. Our work highlights the potential of  $\text{CeO}_2$ -based adsorbents for the removal of  $\text{PO}_4^{3-}$ . The  $\text{CeO}_2\text{-SiO}_2$  developed in this work can be further integrated in separation devices, for example, membranes, filters, and column reactors, to improve treatment and recovery of P-based nutrients from environmental waters.

#### ASSOCIATED CONTENT

# **S** Supporting Information

The Supporting Information is available free of charge on the ACS Publications website at DOI: 10.1021/acsanm.9b01512.

Description of the zeta potential versus pH measurement; surface area measurement; ATR-FTIR and XPS analysis of the as-prepared adsorbent material; adsorption equilibrium isotherm study of  $CeO_2$ – $SiO_2$  material with fitted Langmuir and Freundlich isotherm with the corresponding parameters; pseudo-first- and pseudo-second-order kinetics obtained by using the nonlinear fitting with the corresponding parameters; zeta potential measurement of the regeneration process; and ATR-FTIR spectra of  $CeO_2$ – $SiO_2$  before and after  $PO_4^{3-}$  adsorption for mechanism explanation (PDF)

## AUTHOR INFORMATION

### **Corresponding Author**

\*E-mail: eandrees@clarkson.edu. Fax: +(315) 268 6610. Tel: +(315) 268 2394.

# ORCID ®

Ali Othman: 0000-0002-7960-4995 Silvana Andreescu: 0000-0003-3382-7939

#### Notes

The authors declare no competing financial interest.

# ACKNOWLEDGMENTS

This work was supported in part by NSF Grant 1610281. Also, this work made use of the Cornell Center for Materials Research Shared Facilities, which are supported through the NSF MRSEC program (DMR-1719875). Financial support

Table 1. Comparison of PO<sub>4</sub><sup>3-</sup> Adsorption Capacities of Various Adsorbents

adsorbent	adsorption capacity $(q_{m'} \text{ mg/g})$	adsorbent dosage (g/L)	pН	equilibrium time	removal (%)	ref
magnetic iron oxide NPs	5.0	0.6	6.0	12 h	97	53
magnetite (Fe <sub>3</sub> O <sub>4</sub> )	27.2	1.0	7.0	24 h	85	54
coir-pith activated carbon	7.7	4	6.0	3 h		55
Fe-Zr binary oxide	41.8	1	4.0	2 h	86	56
coir-pith-Fe	70.9	2	3.0	12 h		57
CuFe <sub>2</sub> O <sub>4</sub>	41.3	0.6	2.6	2 h	65	58
amorphous ZrO2 NPs	99	0.1	6.2	8 h	99	59
hydrous niobium oxide	15	2	12	4 h	>88	60
zirconium oxide	30	1.2	6.7	5 h	54	61
hydrous zirconium oxide	66	2	5	8 h	99	62
Fe <sub>3</sub> O <sub>4</sub> @SiO <sub>2</sub> -CeO <sub>2</sub>	26.5	0.5	6	400 min		63
Fe <sub>3</sub> O <sub>4</sub> @SiO <sub>2</sub> @mCeO <sub>2</sub>	64.1	0.7	6	1 h	91	17
$Ce_{0.8}Zr_{0.2}O_2$	112.2	0.1	6.2	1 h	92	30
CeO <sub>2</sub> -SiO <sub>2</sub>	110	2	7.0	1 h	99	this work

provided by the New York State Pollution Prevention Institute through a grant from the New York State Department of Environmental Conservation is also acknowledged.

### REFERENCES

- (1) Cosgrove, W. J.; Loucks, D. P. Water Management: Current and Future Challenges and Research Directions. Water Resour. Res. 2015, 51 (6), 4823-4839.
- (2) Elser, J.; Bennett, E. Phosphorus Cycle: A Broken Biogeochemical Cycle. Nature 2011, 478 (7367), 29-31.
- (3) Canfield, D. E.; Glazer, A. N.; Falkowski, P. G. The Evolution and Future of Earth's Nitrogen Cycle. Science 2010, 330 (6001), 192-
- (4) EPA. National Rivers and Streams Assessment 2008-2009: A Collaborative Survey (Draft); Office of Wetlands, Oceans, and Watersheds, Office of Research and Development, U.S. Environmental Protection Agency: Washington, DC; https://www.epa.gov/ national-aquatic-resource-surveys/nrsa (accessed on 29 October 2014).
- (5) Sharma, L. K.; Bali, S. K.; Zaeen, A. A. A Case Study of Potential Reasons of Increased Soil Phosphorus Levels in the Northeast United States. Agronomy 2017, 7 (4), 85.
- (6) Zhang, L.; Wan, L.; Chang, N.; Liu, J.; Duan, C.; Zhou, Q.; Li, X.; Wang, X. Removal of Phosphate from Water by Activated Carbon Fiber Loaded with Lanthanum Oxide. J. Hazard. Mater. 2011, 190 (1-3), 848-855.
- (7) Awual, M. R.; Jyo, A.; Ihara, T.; Seko, N.; Tamada, M.; Lim, K. T. Enhanced Trace Phosphate Removal from Water by Zirconium-(IV) Loaded Fibrous Adsorbent. Water Res. 2011, 45 (15), 4592-4600.
- (8) Zong, E.; Wei, D.; Wan, H.; Zheng, S.; Xu, Z.; Zhu, D. Adsorptive Removal of Phosphate Ions from Aqueous Solution using Zirconia-Functionalized Graphite Oxide. Chem. Eng. J. 2013, 221, 193-203.
- (9) Jiang, C.; Jia, L.; He, Y.; Zhang, B.; Kirumba, G.; Xie, J. Adsorptive Removal of Phosphorus from Aqueous Solution using Sponge Iron and Zeolite. J. Colloid Interface Sci. 2013, 402 (Supplement C), 246-252.
- (10) Yagi, S.; Fukushi, K. Removal of Phosphate from Solution by Adsorption and Precipitation of Calcium Phosphate onto Monohydrocalcite. J. Colloid Interface Sci. 2012, 384 (1), 128-136.
- (11) Geelhoed, J. S.; Hiemstra, T.; Van Riemsdijk, W. H. Phosphate and Sulfate Adsorption on Goethite: Single Anion and Competitive Adsorption. Geochim. Cosmochim. Acta 1997, 61 (12), 2389-2396.
- (12) Lürling, M.; Waajen, G.; van Oosterhout, F. Humic Substances Interfere with Phosphate Removal by Lanthanum Modified Clay in Controlling Eutrophication. Water Res. 2014, 54, 78-88.
- (13) Othman, A.; Karimi, A.; Andreescu, S. Functional Nanostructures for Enzyme based Biosensors: Properties, Fabrication and Applications. J. Mater. Chem. B 2016, 4 (45), 7178-7203.
- (14) Andreescu, D.; Bulbul, G.; Ozel, R. E.; Hayat, A.; Sardesai, N.; Andreescu, S. Applications and Implications of Nanoceria Reactivity: Measurement Tools and Environmental Impact. Environ. Sci.: Nano **2014**, 1 (5), 445–458.
- (15) Recillas, S.; García, A.; González, E.; Casals, E.; Puntes, V.; Sánchez, A.; Font, X. Preliminary Study of Phosphate Adsorption onto Cerium Oxide Nanoparticles for Use in Water Purification; Nanoparticles Synthesis and Characterization. Water Sci. Technol. **2012**, 66 (3), 503–509.
- (16) Li, C.-m.; Zhang, Y.-s.; Wang, X.-p.; Yin, X.-b.; Luo, N.-n.; Khayambashi, A.; Wei, Y.-z. The Synthesis and Characterization of Hydrous Cerium Oxide Nanoparticles Loaded on Porous Silica Micro-Sphere as Novel and Efficient Adsorbents to Remove Phosphate Radicals from Water. Microporous Mesoporous Mater. 2019, 279, 73-81.
- (17) Ding, H.; Zhao, Y.; Duan, Q.; Wang, J.; Zhang, K.; Ding, G.; Xie, X.; Ding, C. Efficient Removal of Phosphate from Aqueous Solution using Novel Magnetic Nanocomposites with Fe<sub>3</sub>O<sub>4</sub>@SiO<sub>2</sub>

- Core and Mesoporous CeO<sub>2</sub> Shell. J. Rare Earths 2017, 35 (10), 984-
- (18) Lee, S.-H.; Lu, Z.; Babu, S. V.; Matijević, E. Chemical Mechanical Polishing of Thermal Oxide Films using Silica Particles Coated with Ceria. J. Mater. Res. 2002, 17 (10), 2744-2749.
- (19) Fogg, D. N.; Wilkinson, N. T. The Colorimetric Determination of Phosphorus. Analyst 1958, 83 (988), 406-414.
- (20) Sathe, T. R.; Agrawal, A.; Nie, S. Mesoporous Silica Beads Embedded with Semiconductor Quantum Dots and Iron Oxide Nanocrystals: Dual-Function Microcarriers for Optical Encoding and Magnetic Separation. Anal. Chem. 2006, 78 (16), 5627-5632.
- (21) Molinari, M.; Symington, A. R.; Sayle, D. C.; Sakthivel, T. S.; Seal, S.; Parker, S. C. Computer-Aided Design of Nanoceria Structures as Enzyme Mimetic Agents: The Role of Bodily Electrolytes on Maximizing Their Activity. ACS Appl. Bio. Mater. 2019, 2 (3), 1098-1106.
- (22) Khalil, K. M. S.; Elkabee, L. A.; Murphy, B. Formation and Characterization of Different Ceria/Silica Composite Materials via Dispersion of Ceria Gel or Soluble Ceria Precursors in Silica Sols. J. Colloid Interface Sci. 2005, 287 (2), 534-541.
- (23) V., M.; Mody, H. M.; Bajaj, H. C.; Jasra, R. V. Adsorption of Cu<sup>2+</sup> on Amino Functionalized Silica Gel with Different Loading. Ind. Eng. Chem. Res. 2009, 48 (19), 8954-8960.
- (24) Andreescu, D.; Matijević, E.; Goia, D. V. Formation of Uniform Colloidal Ceria in Polyol. Colloids Surf., A 2006, 291 (1), 93-100.
- (25) Pop, O. L.; Diaconeasa, Z.; Mesaroş, A.; Vodnar, D. C.; Cuibus, L.; Ciontea, L.; Socaciu, C. FT-IR Studies of Cerium Oxide Nanoparticles and Natural Zeolite Materials. Bull. Univ. Agric. Sci. Vet. Med. Cluj-Napoca, Food Sci. Technol. 2015, 72 (1), 50-55.
- (26) Wang, X.-D.; Shen, Z.-X.; Sang, T.; Cheng, X.-B.; Li, M.-F.; Chen, L.-Y.; Wang, Z.-S. Preparation of Spherical Silica Particles by Stöber Process with High Concentration of Tetra-Ethyl-Orthosilicate. J. Colloid Interface Sci. 2010, 341 (1), 23-29.
- (27) Antony, R.; David Manickam, S. T.; Kollu, P.; Chandrasekar, P. V.; Karuppasamy, K.; Balakumar, S. Highly Dispersed Cu(II), Co(II) and Ni(II) Catalysts Covalently Immobilized on Imine-Modified Silica for Cyclohexane Oxidation with Hydrogen Peroxide. RSC Adv. 2014, 4 (47), 24820-24830.
- (28) Vivek, S.; Arunkumar, P.; Babu, K. S. In situ Generated Nickel on Cerium Oxide Nanoparticle for Efficient Catalytic Reduction of 4-Nitrophenol. RSC Adv. 2016, 6 (51), 45947-45956.
- (29) Reddy, B. M.; Katta, L.; Thrimurthulu, G. Novel Nanocrystalline  $Ce_{1-x}La_xO_{2-\delta}$  (x=0.2) Solid Solutions: Structural Characteristics and Catalytic Performance. Chem. Mater. 2010, 22 (2), 467-475.
- (30) Su, Y.; Yang, W.; Sun, W.; Li, Q.; Shang, J. K. Synthesis of Mesoporous Cerium-Zirconium Binary Oxide Nanoadsorbents by ASolvothermal Process and Their Effective Adsorption of Phosphate from Water. Chem. Eng. J. 2015, 268, 270-279.
- (31) Singh, S.; Dosani, T.; Karakoti, A. S.; Kumar, A.; Seal, S.; Self, W. T. A Phosphate-Dependent Shift in Redox State of Cerium Oxide Nanoparticles and its Effects on Catalytic Properties. Biomaterials 2011, 32 (28), 6745-6753.
- (32) Wan, J.; Tao, T.; Zhang, Y.; Liang, X.; Zhou, A.; Zhu, C. Phosphate Adsorption on Novel Hydrogel Beads with Interpenetrating Network (IPN) Structure in Aqueous Solutions: Kinetics, Isotherms and Regeneration. RSC Adv. 2016, 6 (28), 23233-23241.
- (33) Almeelbi, T.; Bezbaruah, A. Aqueous Phosphate Removal Using Nanoscale Zero-Valent Iron. J. Nanopart. Res. 2012, 14 (7), 1-
- (34) Li, M. X.; Liu, J. Y.; Xu, Y. F.; Qian, G. R. Phosphate Adsorption on Metal Oxides and Metal Hydroxides: A Comparative Review. Environ. Rev. 2016, 24 (3), 319-332.
- (35) Song, J.; Kong, H.; Jang, J. Adsorption of Heavy Metal Ions from Aqueous Solution by Polyrhodanine-Encapsulated Magnetic Nanoparticles. J. Colloid Interface Sci. 2011, 359 (2), 505-511.
- (36) Do, M. H.; Phan, N. H.; Nguyen, T. D.; Pham, T. T. S.; Nguyen, V. K.; Vu, T. T. T.; Nguyen, T. K. P. Activated Carbon/ Fe<sub>3</sub>O<sub>4</sub>Nanoparticle Composite: Fabrication, Methyl Orange Removal

- and Regeneration by Hydrogen Peroxide. Chemosphere 2011, 85 (8), 1269–1276.
- (37) Damatov, D.; Mayer, J. M. (Hydro)peroxide ligands on colloidal cerium oxide nanoparticles. *Chem. Commun.* **2016**, *52* (67), 10281–10284.
- (38) Ornatska, M.; Sharpe, E.; Andreescu, D.; Andreescu, S. Paper Bioassay Based on Ceria Nanoparticles as Colorimetric Probes. *Anal. Chem.* **2011**, 83 (11), 4273–4280.
- (39) Li, C.; Domen, K.; Maruya, K.-I.; Onishi, T. Oxygen Exchange Reactions over Cerium Oxide: An FT-IR Study. *J. Catal.* **1990**, *123* (2), 436–442.
- (40) Perez, J. M.; Asati, A.; Nath, S.; Kaittanis, C. Synthesis of Biocompatible Dextran-Coated Nanoceria with pH-Dependent Antioxidant Properties. *Small* **2008**, 4 (5), 552–556.
- (41) Lin, J.; Wu, Y.; Khayambashi, A.; Wang, X.; Wei, Y. Preparation of a Novel CeO<sub>2</sub>/SiO<sub>2</sub>Adsorbent and its Adsorption Behavior for Fluoride Ion. *Adsorpt. Sci. Technol.* **2018**, *36* (1–2), 743–761.
- (42) Daou, T. J.; Begin-Colin, S.; Grenèche, J. M.; Thomas, F.; Derory, A.; Bernhardt, P.; Legaré, P.; Pourroy, G. Phosphate Adsorption Properties of Magnetite-Based Nanoparticles. *Chem. Mater.* **2007**, *19* (18), 4494–4505.
- (43) Othman, A.; Dumitrescu, E.; Andreescu, D.; Andreescu, S. Nanoporous Sorbents for the Removal and Recovery of Phosphorus from Eutrophic Waters: Sustainability Challenges and Solutions. *ACS Sustainable Chem. Eng.* **2018**, *6* (10), 12542–12561.
- (44) Kralchevska, R. P.; Prucek, R.; Kolařík, J.; Tuček, J.; Machala, L.; Filip, J.; Sharma, V. K.; Zbořil, R. Remarkable Efficiency of Phosphate Removal: Ferrate(VI)-Induced in Situ Sorption on Core-Shell Nanoparticles. *Water Res.* **2016**, *103* (Supplement C), 83–91.
- (45) Xie, F.; Wu, F.; Liu, G.; Mu, Y.; Feng, C.; Wang, H.; Giesy, J. P. Removal of Phosphate from Eutrophic Lakes through Adsorption by in Situ Formation of Magnesium Hydroxide from Diatomite. *Environ. Sci. Technol.* **2014**, *48* (1), 582–590.
- (46) Xu, J.; Harmer, J.; Li, G.; Chapman, T.; Collier, P.; Longworth, S.; Tsang, S. C. Size Dependent Oxygen Buffering Capacity of Ceria Nanocrystals. *Chem. Commun.* **2010**, *46* (11), 1887–1889.
- (47) Barth, C.; Laffon, C.; Olbrich, R.; Ranguis, A.; Parent, P.; Reichling, M. A Perfectly Stoichiometric and Flat CeO<sub>2</sub>(111) Surface on a Bulk-Like Ceria Film. *Sci. Rep.* **2016**, *6*, 21165.
- (48) Mullins, D.; Overbury, S.; Huntley, D. Electron Spectroscopy of Single Crystal and Polycrystalline Cerium Oxide Surfaces. *Surf. Sci.* **1998**, 409 (2), 307–319.
- (49) Hasegawa, T.; Shahed, S. M. F.; Sainoo, Y.; Beniya, A.; Isomura, N.; Watanabe, Y.; Komeda, T. Epitaxial Growth of CeO<sub>2</sub> (111) Film on Ru (0001): Scanning Tunneling Microscopy (STM) and X-Ray Photoemission Spectroscopy (XPS) study. *J. Chem. Phys.* **2014**, *140* (4), 044711.
- (50) Henderson, M. A.; Perkins, C.; Engelhard, M. H.; Thevuthasan, S.; Peden, C. H. Redox Properties of Water on the Oxidized and Reduced Surfaces of CeO<sub>2</sub> (111). *Surf. Sci.* **2003**, *526* (1), 1–18.
- (51) Duval, Y.; Mielczarski, J. A.; Pokrovsky, O. S.; Mielczarski, E.; Ehrhardt, J. J. Evidence of the Existence of Three Types of Species at the Quartz-Aqueous Solution Interface at pH 0–10: XPS Surface Group Quantification and Surface Complexation Modeling. *J. Phys. Chem. B* **2002**, *106* (11), 2937–2945.
- (52) Xie, J.; Wang, Z.; Lu, S.; Wu, D.; Zhang, Z.; Kong, H. Removal and Recovery of Phosphate from Water by Lanthanum Hydroxide Materials. *Chem. Eng. J.* **2014**, 254, 163–170.
- (53) Yoon, S.-Y.; Lee, C.-G.; Park, J.-A.; Kim, J.-H.; Kim, S.-B.; Lee, S.-H.; Choi, J.-W. Kinetic, Equilibrium and Thermodynamic Studies for Phosphate Adsorption to Magnetic Iron Oxide Nanoparticles. *Chem. Eng. J.* **2014**, 236, 341–347.
- (54) de Vicente, I.; Merino-Martos, A.; Cruz-Pizarro, L.; de Vicente, J. On the Use of Magnetic Nano and Microparticles for Lake Restoration. *J. Hazard. Mater.* **2010**, *181* (1), 375–381.
- (55) Kumar, P.; Sudha, S.; Chand, S.; Srivastava, V. C. Phosphate Removal from Aqueous Solution Using Coir-Pith Activated Carbon. Sep. Sci. Technol. 2010, 45 (10), 1463–1470.

- (56) Long, F.; Gong, J.-L.; Zeng, G.-M.; Chen, L.; Wang, X.-Y.; Deng, J.-H.; Niu, Q.-Y.; Zhang, H.-Y.; Zhang, X.-R. Removal of Phosphate from Aqueous Solution by Magnetic Fe–Zr Binary Oxide. *Chem. Eng. J.* **2011**, *171* (2), 448–455.
- (57) Krishnan, K. A.; Haridas, A. Removal of Phosphate from Aqueous Solutions and Sewage using Natural and Surface Modified Coir Pith. *J. Hazard. Mater.* **2008**, *152* (2), 527–535.
- (58) Tu, Y.-J.; You, C.-F. Phosphorus Adsorption onto Green Synthesized Nano-Bimetal Ferrites: Equilibrium, Kinetic and Thermodynamic Investigation. *Chem. Eng. J.* **2014**, *251*, 285–292.
- (59) Su, Y.; Cui, H.; Li, Q.; Gao, S.; Shang, J. K. Strong Adsorption of Phosphate by Amorphous Zirconium Oxide Nanoparticles. *Water Res.* 2013, 47 (14), 5018–5026.
- (60) Rodrigues, L. A.; da Silva, M. L. C. P. Thermodynamic and Kinetic Investigations of Phosphate Adsorption onto Hydrous Niobium Oxide Prepared by Homogeneous Solution Method. *Desalination* **2010**, 263 (1), 29–35.
- (61) Liu, H.; Sun, X.; Yin, C.; Hu, C. Removal of Phosphate by Mesoporous ZrO<sub>2</sub>. *J. Hazard. Mater.* **2008**, *151* (2), *616–622*.
- (62) Rodrigues, L. A.; Maschio, L. J.; Coppio, L. d. S. C.; Thim, G. P.; Pinto da Silva, M. L. C. Adsorption of Phosphate from Aqueous Solution by Hydrous Zirconium Oxide. *Environ. Technol.* **2012**, 33 (12), 1345–1351.
- (63) Liu, J.; Cao, J.; Hu, Y.; Han, Y.; Zhou, J. Adsorption of Phosphate Ions from Aqueous Solutions by a CeO<sub>2</sub> Functionalized Fe<sub>3</sub>O<sub>4</sub>@SiO<sub>2</sub> Core-Shell Magnetic Nanomaterial. *Water Sci. Technol.* **2017**, 76 (11), 2867–2875.